

Proteomic response of the marine ammonia-oxidising archaeon *Nitrosopumilus maritimus* to iron limitation reveals strategies to compensate for nutrient scarcity

Roxana T. Shafiee ^{1*}, Joseph T. Snow,¹
Svenja Hester,² Qiong Zhang¹ and
Rosalind E. M. Rickaby¹

¹Department of Earth Sciences, South Parks Road,
University of Oxford, Oxfordshire, OX1 3AN, UK.

²Department of Biochemistry, South Parks Road,
University of Oxford, Oxfordshire, OX1 3QU, UK.

Summary

Dissolved iron (Fe) is vanishingly low in the oceans, with ecological success conferred to microorganisms that can restructure their biochemistry to maintain high growth rates during Fe scarcity. Chemolithoautotrophic ammonia-oxidising archaea (AOA) are highly abundant in the oceans, constituting ~30% of cells below the photic zone. Here we examine the proteomic response of the AOA isolate *Nitrosopumilus maritimus* to growth-limiting Fe concentrations. Under Fe limitation, we observed a significant reduction in the intensity of Fe-dense ferredoxins associated with respiratory complex I whilst complex III and IV proteins with more central roles in the electron transport chain remain unchanged. We concomitantly observed an increase in the intensity of Fe-free functional alternatives such as flavodoxin and plastocyanin, thioredoxin and alkyl hydroperoxide which are known to mediate electron transport and reactive oxygen species detoxification, respectively. Under Fe limitation, we found a marked increase in the intensity of the ABC phosphonate transport system (Phn), highlighting an intriguing link between Fe and P cycling in *N. maritimus*. We hypothesise that an elevated uptake of exogenous phosphonates under Fe limitation may either supplement *N. maritimus*' endogenous methylphosphonate biosynthesis pathway - which requires Fe - or enhance the production of

phosphonate-containing exopolysaccharides known to efficiently bind environmental Fe.

Introduction

Ammonia-oxidising archaea (AOA) occupy a diverse array of ecosystems from hot springs to the oligotrophic open ocean. All cultivated AOA, recently placed into the updated class of Nitrososphaeria within the phylum Thermoproteota (Parks *et al.*, 2020; Rinke *et al.*, 2020) perform the first step of nitrification, the central component of the biogeochemical nitrogen (N) cycle, by oxidising ammonium (NH_4^+) to nitrite (NO_2^-). In the oceans, surface water nitrification can account for up to 30% of phytoplankton nitrogen nutrition (Yool *et al.*, 2007) and provides an oxidised nitrogen niche for the large microphytoplankton (such as diatoms) that drive greater carbon export to the deep ocean relative to picophytoplankton such as cyanobacteria (Berg *et al.*, 2003; Fawcett *et al.*, 2011; Glibert *et al.*, 2016). Marine AOA constitute up to 30% of total prokaryotic cells below the photic zone (Kamer *et al.*, 2001) and as such contribute a major fraction of gene copies and transcripts in marine metagenomes and metatranscriptomes (Hollibaugh *et al.*, 2011). Marine AOA also play a role in major biogeochemical cycles through their contribution to the production of nitrous oxide (Freing *et al.*, 2012), methane (Metcalf *et al.*, 2012) and cobalamin (Doxey *et al.*, 2015; Heal *et al.*, 2017).

The success of marine AOA is owed to adaptations which make these microorganisms well suited to the inhospitable open ocean wherein nutrient fluxes are low. Large surface-to-volume ratios (Könneke *et al.*, 2005), a high affinity for NH_4^+ (Martens-Habben *et al.*, 2009), an energy-efficient C-fixation pathway (Könneke *et al.*, 2014), and streamlined genomes with a low proportion of non-coding DNA (Walker *et al.*, 2010; Santoro *et al.*, 2015) make marine AOA oligotrophic-specialists or 'oligotrophs'. In ~30% of surface oceans, low concentrations of dissolved iron (Fe) limit the growth of marine phytoplankton (Moore *et al.*, 2013), but the role of Fe in modulating the growth of non-photosynthetic but environmentally important microbial groups has traditionally

Received 26 October, 2020; accepted 25 March, 2021. *For correspondence. E-mail roxana.shafiee@earth.ox.ac.uk.

received much less attention. Recently we demonstrated that the model AOA isolate *Nitrosopumilus maritimus* strain SCM1, despite possessing a unique Cu-dominated centric biochemistry compared to its ammonia-oxidising bacterial counterparts (Walker et al., 2010; Amin et al., 2013; Shafiee et al., 2021), requires a greater concentration of unchelated Fe (Fe') for growth than many cosmopolitan marine microorganisms (Shafiee et al., 2019). A greater Fe requirement for growth relative to other marine microorganisms suggests that AOA must occupy an Fe-rich niche and indeed aligns with observations of AOA maxima at the base of the photic zone (Santoro et al., 2013; Shiozaki et al., 2016). At this depth, Fe supply is great due to the combined effect of a decrease in competition for Fe (as phytoplankton become light limited) and Fe remineralisation from sinking organic matter. Fe fluxes from remineralisation can be episodic, depending heavily on levels of surface productivity and as such AOA may undergo prolonged periods of Fe starvation between nutrient pulses. Marine microorganisms have evolved a number of strategies to survive Fe scarcity including a reduction in Fe demand by downregulating the expression of Fe-binding proteins (retrenchment); replacing Fe-dense proteins with Fe-free substitutes (La Roche et al., 1996; Erdner et al., 1999; Snow et al., 2015); producing Fe-chelating compounds to enhance access to extracellular Fe (Boiteau et al., 2016) or increasing the transcription or affinity of membrane transporter proteins (Kustka et al., 2007; Allen et al., 2008; Cohen et al., 2018; Maldonado et al., 2006). The biochemical strategies implemented under Fe scarcity can be gleaned from the change in protein expression (proteome) which acts as the basis of developing biomolecular tools to detect Fe limitation in vast expanses of mixed microbial communities *in situ*. For example, the phytoplankton Fe deficiency-induced protein A (IdiA) involved in cellular Fe scavenging has been used as a marker for Fe stress in open ocean field populations (Webb et al., 2001; Saito et al., 2014; Chappell et al., 2015). The application of proteomic biomarkers provides a powerful alternative to traditional nutrient amendment experiments - which often alter community composition and do not necessarily capture the multi-complexed nature of stressors - which can be applied to wide geographic regions.

Here we examine the proteomic response of the model marine AOA isolate, *Nitrosopumilus maritimus* strain SCM1 (herein referred to as *N. maritimus*) to Fe limitation. We present the label-free quantitative intensity profiles of *N. maritimus* under Fe-limited and Fe-replete growth, thereby gaining important insight into the potential mechanisms adopted by AOA to navigate Fe scarcity.

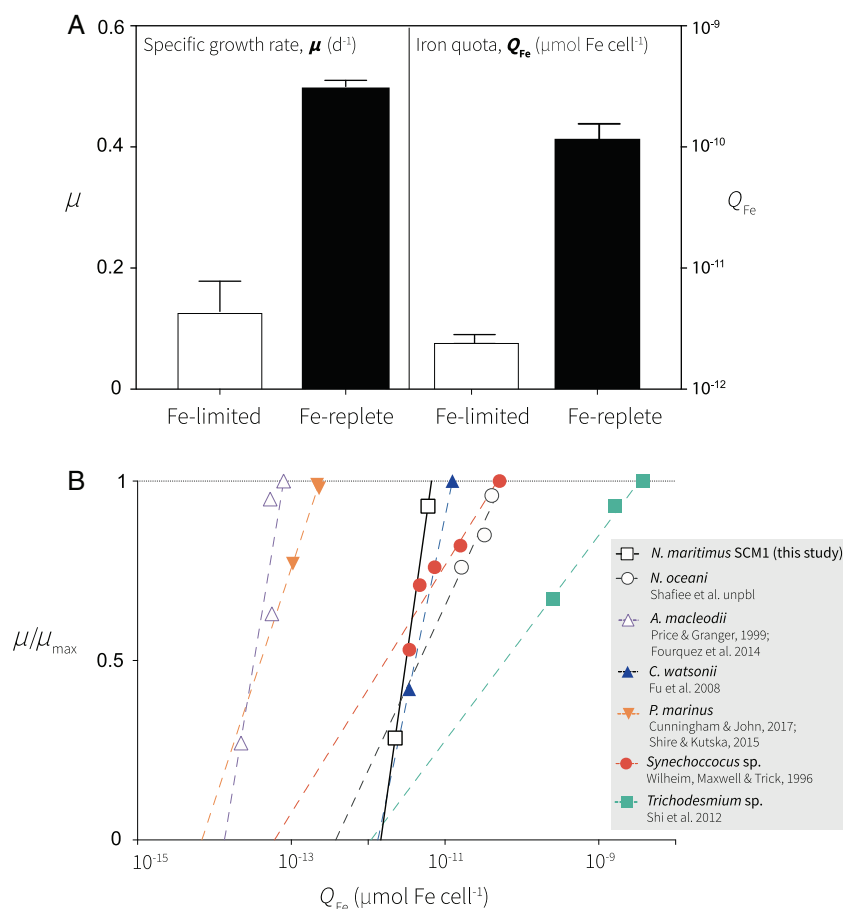
Results and discussion

Growth rates, cellular Fe quota and protein detection

Low concentrations of unchelated iron ([Fe']) led to a 59% reduction in specific growth rate (μ) and a decline in final nitrite (NO_2^-) concentration from 913 to 185 $\mu\text{mol L}^{-1}$ (Fig. 1; Supplementary Fig. 1) between treatments. In Fe-replete *N. maritimus* we measured an intracellular-Fe quota of $1.1 \times 10^{-10} \mu\text{mol Fe cell}^{-1}$ ($\pm 4.2 \times 10^{-11}$) which reduced to $2.25 \times 10^{-12} \mu\text{mol Fe cell}^{-1}$ ($\pm 3.9 \times 10^{-13}$) in Fe-limited cells (Fig. 1). Of the 1795 predicted protein-encoding genes in the *N. maritimus* genome (www.jgi.doe.gov), 1346 discrete proteins were detected in the Fe-replete proteome (74.9%) and 1337 proteins in the Fe-limited proteome (74.5%) (at a 1% FDR). Biological replicates showed strong reproducibility with r^2 values exceeding 0.8 in all comparisons (Supplementary Fig. 2). The detected proteome coverage was greater or consistent with previous proteomic recovery of *N. maritimus* (68% in Bayer et al., 2019; 74% in Qin et al., 2018) and *Candidatus Nitrosopelagicus brevis* (~70% in Santoro et al., 2015) and supports the notion that AOA have streamlined genomes with a high proportion of predicted protein expression. Sixty-nine proteins showed a significant difference in label-free quantitation (LFQ) intensity between Fe treatments (FDR adjusted p -value < 0.05). All differential protein intensities discussed in this study are statistically significant at an FDR-adjusted p -value < 0.05 . Relative to the Fe-replete treatment, 34 proteins increased significantly in LFQ intensity and 35 decreased in intensity in the Fe-limited treatment. Three proteins that were detected in the Fe-limited proteome were absent in all replicates (or below L.O.D.) of the Fe-replete proteome, whereas 12 proteins were detected in the Fe-replete proteome that was absent from all replicates of the Fe-limited proteome (Supplementary Table 1). Proteins with predicted functions in the S-layer (Nmar_1547), ammonia oxidation (Nmar_1102), carbon fixation (Nmar_0273) and genetic information processing (Nmar_1034) showed the highest LFQ intensities in both Fe-limited and Fe-replete proteomes (Table 1).

Ammonia monooxygenase

Ammonia-monooxygenase (AMO), the hallmark enzyme of ammonia-oxidising microorganisms, is comprised of three subunits: AmoA, B and C (Nmar_1500, Nmar_1503, Nmar_1502). Under Fe limitation, AMO subunit LFQ intensity increased as a proportion of total signal from 1.75% to 2.37% with AmoB among the top 10 most intense proteins in the Fe-limited proteome (Table 1). Additionally, we found that AmoA (Nmar_1500) intensity increased with statistical significance in Fe-limited treatments - suggesting that *N. maritimus*' core ammonia



oxidation machinery remains intact even when Fe is scarce. This highlights that the availability of the AMO complex may not be the rate-limiting factor which leads to the observed decline in ammonia oxidation rate when Fe' is low (Fig. 1, Supplementary Fig. 1). In contrast, energy and Cu limitation reduces the transcription of all AMO subunits (Qin *et al.*, 2018; Reyes *et al.*, 2020), apart from *amoC* which is preferentially retained under NH₄⁺ starvation (Qin *et al.*, 2018). The ostensible greater impact of Cu and NH₄⁺ limitation on the AMO complex may be expected given the larger predicted Cu requirement of AMO (based on AMO homology to methane monooxygenase) and the fact NH₄⁺ is required as its substrate: AmoC and AmoA putatively bind 7 Cu atoms collectively compared to AmoB which only requires 3 Fe atoms. However, it cannot be ruled out that transcriptional changes under Fe limitation are not apparent at the proteomic level due to differential rates of post-translational protein degradation. This potential is highlighted by the divergence in AMO subunit abundance between metatranscriptomic and metaproteomic analyses: marine *amoC* and *amoA* transcripts typically outnumber *amoB* transcripts in metatranscriptomes (Feike

et al., 2012; Shi *et al.*, 2012) but initial metaproteomic surveys show that *Nitrosopumilus*-like AmoA and AmoB proteins are ~three-fold more abundant and widespread compared with AmoC (Saunders *et al.*, unpubl; Saito *et al.*, 2020; Supplementary Fig. 3). This disparity highlights the importance of complementary proteomic and transcriptomic characterisation of AMO stoichiometry in future research.

Ammonia oxidation and the electron transport chain

In Fe-replete treatments, Complex I proteins were among the most intensely detected proteins in the *N. maritimus* proteome (Table 1) and are also predicted to be the most Fe dense based on our analysis of Fe-binding proteins in *N. maritimus*' genome-predicted proteome (Supplementary Table 1; See *Biological function groups and Fe containing proteins*). Complex I and putatively associated ferredoxins require a predicted 16 atoms of Fe compared with AmoC, complex III and complex IV which we predict in total require only 11 Fe atoms (Supplementary Table 1). Complex I is responsible for the generation of

Table 1. Top 10 most intense proteins based on LFQ intensities in Fe-replete and Fe-limited treatments, based on LFQ intensity.

	Protein	Biological function group	Protein description	LFQ intensity	Percentage of total intensity
Fe-limited <i>N. maritimus</i> 250 pmol L ⁻¹ Fe'	Nmar_1547	S-layer, cell wall & membrane	Uncharacterised protein	1.9×10^{11}	19.0
	Nmar_0875	ABC transporters	Phosphonate ABC transporter, periplasmic phosphonate-binding protein	5.2×10^{10}	5.3
	Nmar_1034	Genetic information processing	Elongation factor 1-alpha	3.3×10^{10}	3.4
	Nmar_0478	Uncharacterised protein	Uncharacterised protein	1.6×10^{10}	1.6
	Nmar_1622	Carbon fixation	Alcohol dehydrogenase zinc-binding domain protein	1.4×10^{10}	1.4
	Nmar_0331	Uncharacterised protein	ABC-3 protein	1.3×10^{10}	1.3
	Nmar_0559	Metabolism (other)	Trans-sialidase	1.2×10^{10}	1.2
	Nmar_0273	Carbon fixation	Carbamoyl-phosphate synthase L chain ATP-binding	1.1×10^{10}	1.1
	Nmar_1503	Ammonia-oxidation/assimilation/N-processing	Ammonia monooxygenase B (AMO)	1.1×10^{10}	1
	Nmar_1102	Ammonia-oxidation/assimilation/N-processing	Blue (Type 1) copper domain protein	1×10^{10}	1
Fe-replete <i>N. maritimus</i> 1050 pmol L ⁻¹ Fe'	Nmar_1547	S-layer, cell wall & membrane	Uncharacterised protein	2.2×10^{11}	21.8
	Nmar_1034	Genetic information processing	Elongation factor 1-alpha	3.3×10^{10}	3.4
	Nmar_1537	Ammonia-oxidation/assimilation/N-processing	4Fe-4S ferredoxin iron-sulfur binding domain protein	2.7×10^{10}	2.6
	Nmar_1622	Carbon fixation	Alcohol dehydrogenase zinc-binding domain protein	1.6×10^{10}	1.6
	Nmar_0239	Ammonia-oxidation/assimilation/N-processing	4Fe-4S ferredoxin iron-sulfur binding domain protein	1.3×10^{10}	1.3
	Nmar_1691	Ammonia-oxidation/assimilation/N-processing	ATP synthase alpha chain	1.1×10^{10}	1.1
	Nmar_1102	Ammonia-oxidation/assimilation/N-processing	Blue (Type 1) copper domain protein	1.1×10^{10}	1
	Nmar_1577	Protein folding/Chaperones	Thermosome	1×10^{10}	1
	Nmar_0273	Carbon fixation	Carbamoyl-phosphate synthase L chain ATP-binding	1×10^{10}	1
	Nmar_1638	S-layer, cell wall & membrane	Uncharacterised protein	1×10^{10}	1

NAD(P)H - a reducing agent involved in numerous cellular processes including nutrient assimilation, biosynthesis, carbon fixation and metabolism. In Fe-limited treatments, we observed a significant reduction in the intensity of complex I proteins and ferredoxins (Nmar_0279; Nmar_0284; Nmar_1765; Nmar_1537, Nmar_0239) but no change in intensity of Fe-containing complexes III and IV or AmoC (Fig. 2). Complex III and *amoC* transcripts were also retained in *N. maritimus* under energy and nutrient limitation (Qin *et al.*, 2018), pointing to their crucial roles in generating a proton motive force and stabilising the AMO holoenzyme under resource limitation. Qin and colleagues also found ferredoxins (specifically Nmar_1765 and Nmar_0239) to be among the most downregulated genes under Cu and NH₄⁺ limitation (Supplementary Fig. 4). This suggests that the eschewal of Fe-containing ferredoxins may be a general, rather than an Fe-specific, limitation response (Supplementary Table 1). This assumes that the reduced

intensity of ferredoxins in our study is primarily underpinned by a downregulation of ferredoxin genes as opposed to differential protein degradation rates between Fe treatments. In Fe-limited treatments we also observed a significant increase in the LFQ intensity of riboflavin synthase (Nmar_1617), flavodoxin (Nmar_1356) and a putative Cu-binding plastocyanin-like protein (Nmar_0815) suggesting that when starved for Fe, *N. maritimus* may functionally replace ferredoxins for Fe-free electron carriers as has been observed in numerous marine microorganisms under Fe limitation (La Roche *et al.*, 1996; Peers and Price, 2006; Snow *et al.*, 2015; Sepúlveda Cisternas *et al.*, 2018). Both flavodoxin (Nmar_1356) and the Cu-binding plastocyanin-like protein (Nmar_0815) are downregulated in response to Cu limitation in *N. maritimus* (Qin *et al.*, 2018) thereby suggesting that these proteins may potentially form part of a Fe-specific limitation response (Supplementary Fig. 4).

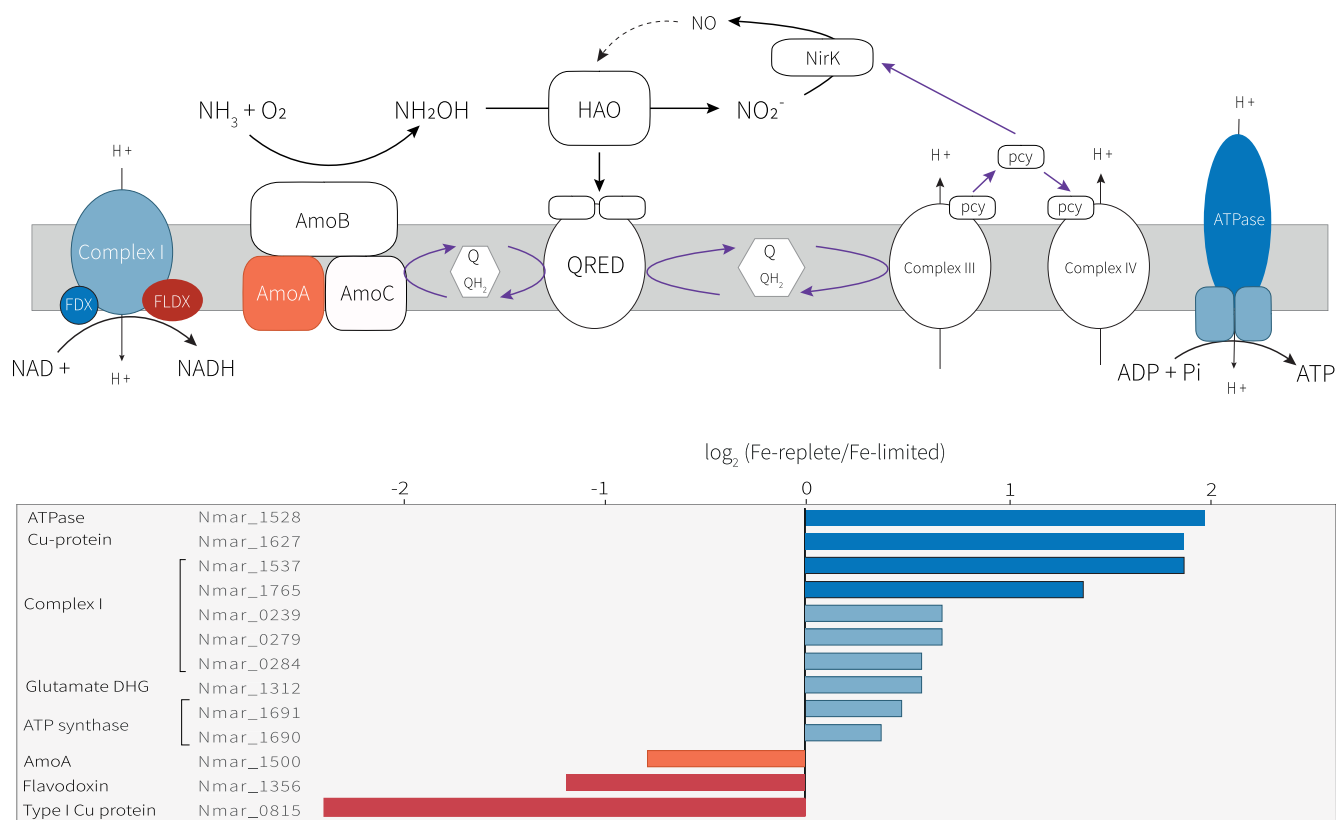


Fig. 2. Proteins involved in the electron transport chain of *N. maritimus*, with proteins showing significant log₂-fold changes (FDR-adjusted *p*-value <0.05) between Fe-replete and Fe-limited proteome shown in colour, corresponding to bar chart below. Abbreviations: pcy: plastocyanin; FDX: Ferredoxin; FLDX: Flavodoxin, QRED: quinone reductase. Purple arrows indicate possible electron flow.

Taken together, we posit that a reduction in Complex I ferredoxins and the potential substitution with Fe-free electron carriers, combined with the retention of Complex III and IV proteins, and AmC presents a compensatory strategy designed to most efficiently reduce Fe demand while keeping energy production as intact as possible. A comparable compensatory strategy has been observed in cosmopolitan marine phytoplankton such as *Trichodesmium* (Shi *et al.*, 2007; Snow *et al.*, 2015). Yet despite such functional replacements, there is still a significant decline in growth rate under low Fe (Fig. 1A) suggesting that such potential functional substitution is not perfect and/or that the rate of Fe uptake is still insufficient under low Fe' to meet the lowered Fe demand - signalling *N. maritimus*' integral need for greater extracellular [Fe'] to maintain a high growth rate.

Carbon fixation, TCA cycle and biosynthesis

The HP/HB cycle adopted by *N. maritimus* to fix carbon contains only one predicted Fe-binding protein (Nmar_1110), which we did not find to change

significantly in intensity between Fe treatments. In contrast, we found that several predicted Fe-containing and Fe-free proteins involved in the TCA cycle and biosynthesis processes changed significantly in intensity between Fe treatments (expanded discussion below). Taken together, this supports the previous notion that Fe-retrenchment targets the processes which are densest in their Fe-use allowing *N. maritimus*' carbon-fixing capacity to remain intact.

In Fe-limited treatments, we observed significant changes to the intensity of proteins involved in the TCA cycle and biosynthesis indicating the presence of potential strategies to mitigate the effects of Fe depletion (Fig. 3). The TCA cycle is central to metabolism - releasing stored energy through the oxidation of acetyl-CoA and providing essential intermediates for biosynthesis. In marine phytoplankton, TCA intermediates are estimated to account for one-third of the total Fe requirement (Raven, 1988) and must be substituted for Fe-free alternatives under low Fe (Cohen *et al.*, 2018). Enzymes with Fe-containing and Fe-free variants include fumarate hydratases and fructose biphosphate aldolases

(Horecker *et al.*, 1972; Picaud *et al.*, 2011). *N. maritimus* only has the genetic capability to produce the Fe-free variants of these enzymes indicating that the TCA cycle already has a parsimonious Fe demand irrespective of extracellular Fe. In Fe-limited treatments we observed a significant drop in intensity of a ferredoxin (Nmar_0413) predicted to mediate the breakdown of pyruvate to acetyl-CoA - a key step in acetyl-CoA supply to the TCA cycle (Fig. 2). Concurrently 4-hydroxy-2-oxovalerate aldolase (Nmar_0149), which supplies pyruvate to Nmar_0413 and Nmar_0414 from the breakdown of pentanoic acid, increased in intensity (Fig. 2). Considered together, we speculate that in order to compensate for the decline in ferredoxins under Fe limitation, *N. maritimus* may instead increase substrate supply (pyruvate) to the ferredoxins - thus saturating these enzymes with pyruvate and in doing so maintaining crucial acetyl-CoA supply to the TCA cycle under Fe limitation.

Detoxification of reactive oxygen species

In addition to their role in ammonia oxidation and the TCA cycle, ferredoxins participate in cellular defence against oxidative stress (Krapp *et al.*, 1997), signifying the potential for a reduced capacity of Fe-limited *N. maritimus* to deal with oxidative stress. Additionally, the breakdown of Fe-S proteins under Fe limitation has been shown to directly generate excess oxidative stress (Liochev and Fridovich, 1994; Keyer and Imlay, 1996; Jang and Imlay, 2010). Therefore in our study, the breakdown of Fe-S clusters is implied by a significant reduction in the intensity of both Fe-containing proteins throughout the cell and the Suf protein family which are responsible for Fe-S cluster biosynthesis and repair (Supplementary Fig. 5: Nmar_0516; Nmar_0496; Nmar_0495). The potential for increased oxidative stress in Fe-limited cells is suggested by a significant increase in Nmar_1386 intensity, a protein annotated as RadA (Supplementary Fig. 5), shown to be responsible for DNA damage repair across the archaeal domain (Komori *et al.*, 2000; Seitz and Kowalczykowski, 2000). RadA was also found to increase significantly in the proteomes of AOA exposed to H₂O₂ (Bayer *et al.*, 2019). We observed a concomitant increase in the intensity of proteins showing homology to Fe-free detoxification proteins thioredoxin reductase (Nmar_0672) and alkyl hydroperoxide (Nmar_1252). This suggests that *N. maritimus* may be reconfiguring its detoxification mechanisms to Fe-free alternatives - a common strategy employed by Fe-limited microorganisms to mitigate enhanced oxidative stress (Holmes *et al.*, 2005; Yingping *et al.*, 2014). We also found that a protein belonging to the universal stress family of proteins, UspA (Nmar_1659) showed a significant 1.7 log₂ fold increase in intensity in Fe-limited treatments

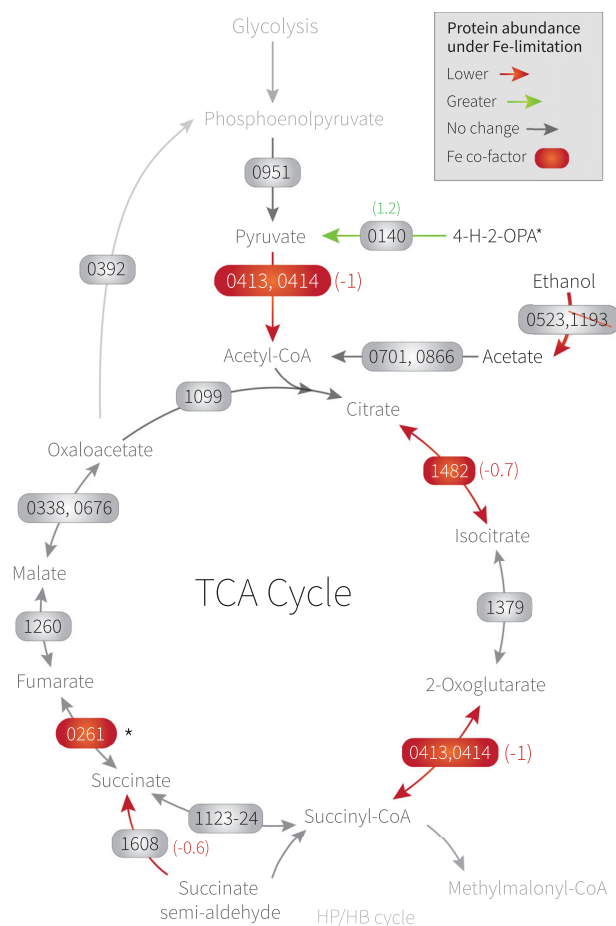


Fig. 3. Tricarboxylic acid cycle in *N. maritimus*. Protein names are shown without 'Nmar' prefix. Proteins showing a significant increase (FDR-adjusted p -value <0.05) in LFQ intensity in Fe-limited treatments are indicated with a green arrow and those showing a significant decrease in LFQ intensity ($p < 0.05$) are indicated with a red arrow (For definition of significance refer to *Data analysis pipeline*). Log₂-fold changes are shown in brackets. Proteins in red are Fe containing based on metalPDB analysis (refer to *Iron allocation in proteome*).

(Supplementary Fig. 5). UspA proteins in *E. coli* play a role in defence against superoxide-generating agents and in cell growth retardation during the stationary phase (Nyström and Neidhardt, 1994; Nachin *et al.*, 2005). However, Bayer *et al.* (2018) found that UspA family proteins were almost completely absent in cultures exposed to H₂O₂ in *N. maritimus*, increasing in abundance only when grown in co-culture with a heterotrophic bacterium or supplemented with catalase - suggesting that UspA is regulated by something other than general, cellular oxidative stress. As *uspA* (Nmar_1659) was found to be down-regulated in response to Cu and NH₄⁺ limitation by Qin *et al.* (2018), we postulate that this UspA family protein may function as an Fe-specific response protein although its exact role in protecting against Fe-induced stress remains to be explored.

S-layer proteins

In both Fe treatments, Nmar_1547 shows the greatest LFQ intensity in the *N. maritimus* proteome, contributing 18.9%–21.7% of all intensities (Table 1), consistent with previous work finding that S-layer proteins (SLP) dominate expressed proteomes (Santoro *et al.*, 2015; Qin *et al.*, 2018; Bayer *et al.*, 2019). Nmar_1547 forms part of the distinctive surface layer (S-layer) of *N. maritimus* and other archaea (Sara and Sleytr, 2000; Urakawa *et al.*, 2011; Santoro *et al.*, 2015) and is a substantial proportion of environmental marine AOA metatranscriptomes and metaproteomes (Hollibaugh *et al.*, 2011; Saunders *et al.*, unpubl.). The S-layer serves as the first selective barrier between the cell interior and the environment which includes interactions with proteins, nutrients and energy substrates (Rodrigues-Oliveira *et al.*, 2017). The chemical properties of the S-layer are hypothesised to enhance *N. maritimus*' access to its energy substrate (NH_4^+) and the micronutrient copper (Cu) (Gorman-Lewis *et al.*, 2014, 2019; Li *et al.*, 2018). The key role played by the S-layer in nutrient and energy acquisition sheds clarity on why there is a significant proteomic investment in S-layer biosynthesis. However, we did not observe any significant change in intensity of detected S-layer proteins, signalling that the S-layer does not respond to changing Fe.

Iron reductase activity and ABC transport

Spatially, following the S-layer, transmembrane proteins are the next selective barrier between the *N. maritimus* cell interior and external environment. In response to Fe limitation, microorganisms may implement numerous strategies to enhance access to extracellular Fe including altering the number or composition of transmembrane proteins, secreting compounds which solubilise inaccessible Fe, or increasing the activity of ferrireductases. The genome of *N. maritimus* has little diversity in metal transport proteins, consistent with characterised oligotrophs (Hogle *et al.*, 2016) and further supports genome streamlining in AOA (Santoro *et al.*, 2015). The majority of AOA isolates, including *N. maritimus*, only encode general cation transporters (Walker *et al.*, 2010; Amin *et al.*, 2013; Shafiee *et al.*, 2019) which were not found to change in intensity under Fe limitation (Fig. 4). Physiological experiments indicate that *N. maritimus* reduces Fe^{3+} to Fe^{2+} prior to uptake (Shafiee *et al.*, 2019), but the ferric reductase protein responsible has yet to be identified. One of the only Fe-containing proteins to increase in intensity under Fe limitation was Nmar_0679, currently annotated as a haem and Fe-S binding sulphite reductase. Sulphite reductases have been shown to reduce a broad range of Fe-chelated substrates via a similar

mechanism to NAD(P)H:flavin oxidoreductase (Coves *et al.*, 1993). If Nmar_0679 is indeed responsible for the Fe-reductase activity in *N. maritimus*, its elevated intensity in response to Fe limitation may signal a potential strategy to increase the bioavailability of dissolved Fe to the cell transporters.

In Fe-limited treatments, several components of the ABC phosphonate transporter (PhnCDE) increased significantly in LFQ intensity (Nmar_0250, Nmar_0874, Nmar_0875) or were only detected in Fe-limited treatments (Nmar_0876 - Fig. 4). Furthermore, a putative transcriptional regulator in the same operon as the phosphate PstSCAB transport system (Nmar_0478) shows the greatest \log_2 fold increase in intensity out of all analysed proteins by an order of magnitude (Fig. 4). Out of these proteins, PhnD (Nmar_0875) and the putative transcriptional regulator of the phosphate PstSCAB transport system (Nmar_0478) show the greatest LFQ intensity in Fe-limited cultures, individually representing 5% and 1.5% of all signal respectively (Table 1). Previous work has shown that *phnD* is downregulated under Cu limitation and NH_4^+ starvation in *N. maritimus* (Qin *et al.*, 2018), and that Phn proteins decrease in abundance in numerous *Nitrosopumilus*-strains upon exposure to H_2O_2 (Bayer *et al.*, 2019). Therefore, we suggest that the significant increase in PhnD intensity observed in our study may be a Fe-specific limitation response (Supplementary Fig. 4; Supplementary Table 1). Phosphonates can be a significant source of phosphorus (P) to microbial communities starved of inorganic P (Cook *et al.*, 1978; Clark *et al.*, 1999; Dyhrman *et al.*, 2006). As *N. maritimus* does not possess proteins with known C-P lyase activity and inorganic P limitation is not alleviated by supplementation with phosphonates (Metcalf *et al.*, 2012; Walker *et al.*, 2010), a link between Fe limitation and P nutritional status is unlikely. An analysis of the spent media from *N. maritimus* cultures shows that *N. maritimus* produces weak ligands as by-products of natural growth - biomaterials hypothesised to be similar to exopolysaccharides (EPS) (Amin *et al.*, 2013). EPS are effective scavengers of cations such as $\text{Fe}^{2+}/\text{Fe}^{3+}$ (Hassler *et al.*, 2011; Hasslet *et al.*, 2015; Gutierrez *et al.*, 2012) owing in part to the negative charge carried by P-bearing groups of the EPS (Ozdemir *et al.*, 2003). P-bearing functional groups have been thermodynamically characterised in Cu^{2+} complexation at the *N. maritimus* cell surface (Gorman-Lewis *et al.*, 2019) and are proposed to be due to the presence of EPS-associated methylphosphonate, which is produced endogenously by *N. maritimus* (Metcalf *et al.*, 2012). The hallmark enzyme of methylphosphonate (Mpn) biosynthesis in *N. maritimus*, methylphosphonic acid synthase (MpnS), binds two Fe atoms (Metcalf *et al.*, 2012) and the final step in the pathway requires free Fe^{2+} as an

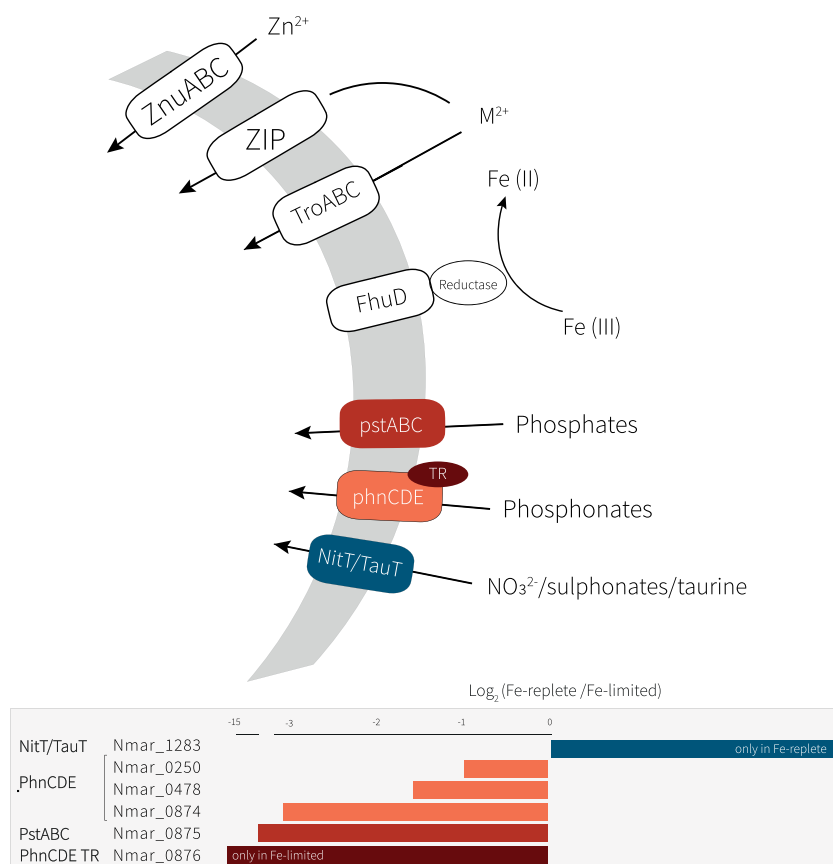


Fig. 4. Proteins involved in membrane transport encoded by *N. maritimus* genome, with proteins showing significant log₂-fold changes in LFQ intensity between Fe-replete and Fe-limited treatments shown in colour. Protein colour on schematic corresponds to the bars on the plot below.

electron donor (Supplementary Fig. 6). We speculate that the observed increase in PhnCDE intensity under Fe limitation may represent a strategy to enhance the uptake of exogenous phosphonates thereby compensating for a reduction in the cell's own methylphosphonate biosynthesis capacity which relies on Fe. While we did not observe any significant change in intensity to proteins of the *N. maritimus*' putative Mpn biosynthesis pathway (Supplementary Fig. 6A), recent analyses of AOA *mpnS* gene biogeography (Qin *et al.*, 2020) highlights the potential for Fe to play a role in regulating Mpn production by acting as a selective pressure for the presence of *mpnS* genes in AOA populations which warrants further investigation. The analysis showed that *mpnS* genes are enriched in open-ocean AOA populations in the mesopelagic (>200 m) relative to surface waters (<200 m), thereby mirroring profiles of dissolved Fe which show an increase in concentration with depth (Supplementary Fig. 7). Based on the results presented in this study, it may be expected for *phnD* gene abundance to follow an inverse trend to *mpnS* abundance, showing an enrichment in shallow AOA populations wherein Fe is scarce relative to deeper populations which have excess to more plentiful Fe. To test this hypothesis, we performed a similar analysis to Qin *et al.* (2020) using the TARA oceans database

to investigate the trend in *phnD: amoA* with depth (see Supplementary Materials for full details). We found that *phnD: amoA* copies per cell in shallow water samples (<200 m) were statistically indistinguishable (Wilcoxon test, $p > 0.05$) from mesopelagic samples (>200 m) (Supplementary Fig. 8; Supplementary Table 1). However, we found that shallow water *phnD: amoA* showed greater variance compared with deep samples (Levene's test, f -ratio value = 16.4, p -value <<0.01) - with *phnD: amoA* ranging over three orders of magnitude below 200 m (Supplementary Fig. 8). A greater variance in *phnD: amoA* in shallow water AOA communities is consistent with the high variability in dissolved Fe concentrations in the surface waters compared with depth (Supplementary Fig. 7), driven by more intensive biogeochemical cycling of Fe in the surface water. Additional analyses would be required to rule out that *mpnS* and *phnD* gene biogeography is not driven by other physio-chemical factors or ecological factors, such as the dominance of deep-water ecotypes (WCB) at depth (Santoro *et al.*, 2019).

An alternative hypothesis is that the marked increase of PhnCDE intensity under Fe limitation is to drive greater phosphonate uptake as a means of enhancing (not compensating for) *N. maritimus*' methylphosphonate production - potentially explaining why methylphosphonate

biosynthesis proteins remain unchanged in response to Fe limitation. In doing so, more P-bearing groups may be provided to the EPS making the cell surface more chemically attractive to extracellular Fe (Supplementary Fig. 6C and D). We speculate that increased Fe binding to P-bearing functional groups on the *N. maritimus* cell surface could provide more Fe substrate to *N. maritimus*' ferric reductase, consistent with an increase in the intensity of the aforementioned ferric reductase candidate under Fe limitation (Nmar_0679). In both instances these conjectures highlight that a more detailed characterisation of EPS of *N. maritimus* and its relationship with Fe cycling and phosphonates is required to robustly explain the increase in PhnCDE under Fe limitation observed in our study.

Conclusion

When growth is limited by Fe, *N. maritimus* primarily minimises Fe demand by reducing Fe-dense ferredoxins which putatively interact with Complex I to generate the reduced co-factor NAD(P)H, potentially functionally substituting these ferredoxins for Fe-free alternatives. In doing so, Fe-binding proteins which play a more central role in electron transfer and ammonia oxidation can be preferentially retained, allowing *N. maritimus* to continue in supporting key energy-yielding pathways under Fe limitation. We observed additional compensatory strategies within the TCA cycle, biosynthesis and detoxification demonstrating efforts to maintain the activity of these pathways whilst significantly reducing Fe requirements. Furthermore, in response to Fe limitation we observed a significant increase in the intensity of proteins with a putative role in the uptake of exogenous phosphonates. We speculate this reflects a potential strategy to enhance or compensate for a reduction in *N. maritimus*' endogenous methylphosphonate biosynthesis pathway which requires Fe-binding proteins.

Experimental procedures

Nitrosopumilus maritimus cultures and growth media

Polycarbonate culture vessels and culturing apparatus were acid cleaned (10% HCl vol./vol., 24 h) and UV sterilised prior to use. Triplicate cultures of *N. maritimus* strain SCM1 (herein referred to as *N. maritimus*) were grown in modified SCM medium (Könneke *et al.*, 2005) buffered with HEPES at pH 7.5 and maintained at 28°C in the dark. Basal salt medium and macronutrients were treated with Chelex® 100 chelating ion exchange resin (BioRad, Watford, UK) to remove trace metal contaminants (Price *et al.*, 1989) and passed through an acid-washed (10% HCl as before) 0.1 µm polycarbonate filter

to sterilise in a metal-free clean laboratory. *Nitrosopumilus maritimus* was cultured at inorganic Fe concentrations ($[Fe']$) previously shown to be limiting (250 pmol L⁻¹ Fe') and replete (1050 pmol L⁻¹ Fe') to growth (Shafiee *et al.*, 2019) but without promoting excess Fe storage. Ethylenediamine tetraacetic acid (Merck, Darmstadt, Germany) (final concentration 12 µmol L⁻¹) was used to buffer Fe and other metals in cultures; $[Fe']$ was controlled by varying the addition of FeCl₃ from filter-sterilised concentrated stocks made using >99.999% trace metal basis salts (Sigma-Aldrich, UK). $[Fe']$ in cultures was calculated using Visual Minteq software (Gustafsson, 2010), including background Fe contamination of 50 nmol L⁻¹ from basal SCM medium with included macronutrients and vitamins but without added trace metals - this was determined using inductively coupled plasma mass spectrometry (ICP-MS) as described by Zhang *et al.* (2018). Cultures were acclimated to limiting and replete $[Fe']$ by transferring cultures consecutively into new media until specific growth rates (μ) did not vary with statistical significance (ANOVA, $p < 0.05$). Growth was determined by measuring concentrations of nitrite ($[NO_2^-]$) spectrophotometrically over time (Griess, 1879), which correlates with cell counts even at low $[Fe']$ (Shafiee *et al.*, 2019). Specific growth rate (d⁻¹) was calculated over the linear phase of semi-log plots of nitrite concentration over time. Differences in specific growth rate (μ) between 250 and 1050 pmol L⁻¹ Fe' treatments were tested for statistical significance using a two-tailed student's *T*-test in Minitab software (version 19.2020.2.0).

Cellular iron and phosphorus quota

All samples and reagents were processed using trace-metal clean techniques and in acid-washed plastic wear (10% HCl v/v, 24 h) in a clean laboratory prior to trace element analysis. *N. maritimus* cells cultured in 2L triplicates at 250 and 1050 pmol L⁻¹ Fe' were harvested in mid-exponential phase by centrifugation at 5000g for 40 min at 4 °C. Cell pellets of each replicate were divided into sub-samples for further trace metal analysis and proteomic analysis (cells for protein extraction were stored at -80°C prior to protein extraction). For trace metal analysis, cell pellets were washed three times with chelexed-SCM basal salt media, which has shown to be effective in removing weakly bound surface (Zhang *et al.*, 2018; Shafiee *et al.*, 2019). Cells were digested in acid-cleaned Teflon as follows: refluxing at 100°C with 16 N quartz distilled (q.d.) HNO₃ (produced in-house) and H₂O₂ (ROMIL UpA™, Cambridge, UK) in a ratio of 3:2 overnight. The liquid was then allowed to evaporate to dryness and 2% q.d. HNO₃ was added to reflux for an hour to resuspend the dried samples. ⁵⁶Fe and ³¹P

concentrations were determined using a Quadrupole ICP-MS Perkin Elmer NexION 350 with Elemental Scientific Flow Injection Auto-sampler (FIAS) in a method optimised for high salt matrixes (Zhang *et al.*, 2018). Per cell Fe quotas were calculated based on the relationship between NO_2^- and cell counts delineated in Shafiee *et al.* (2019).

Protein extraction

Prior to protein analysis frozen cell pellets were thawed on ice, then lysed by sonication in 10×10 s bursts (Hielscher UP200S ultrasonic processor, 70% amplitude) in 1 ml of 0.5% SDS/0.5% Triton extraction buffer (on ice). A 0.5% SDS/0.5% Triton extraction buffer (in a base of 20 mM Tris-Cl, pH 8) was predetermined to be the most effective detergent ratio for protein extraction from a range of buffer combinations in preliminary extraction experiments using *N. maritimus* cells (Supplementary Fig. 9). Pierce BCA protein assay kit (Thermo Fisher Scientific, UK) was used to determine protein concentration following extraction, using the same matrix as the protein extraction buffer. Protein concentration in extracts ranged between $0.6 \mu\text{g} \mu\text{l}^{-1}$ in Fe-limited samples to $1.42 \mu\text{g} \mu\text{l}^{-1}$ in Fe-replete cells. Forty micrograms of protein digest from each biological replicate was used for subsequent proteolytic digestion and detergent removal.

SP3 protocol

Proteolytic digestion and detergent removal from the cell lysate was performed using a single-pot, solid-phase-enhanced sample preparation protocol (Hughes *et al.*, 2019). Proteins in extraction buffer were denatured in 8 M urea (prepared in 100 mM ammonium bicarbonate buffer) at room temperature (RT) for 30 min. Disulphide bridges were reduced with Bond-Breaker™ TCEP Solution (Thermo Scientific) to a final concentration of 10 mM at RT for 30 min, followed by the addition of freshly prepared 2-chloroacetamide (in 100 mM ammonium bicarbonate buffer - final concentration 50 mM) at RT for 30 min in the dark. Protein sample was added to 100 μg of prepared Sera-Mag™ SpeedBeads™ Carboxylate-Modified Magnetic Particles (Sigma-Aldrich). In brief, magnetic particles were prepared by forming a slurry with HPLC grade MilliQ water (beads:MilliQ ratio of 1:4), allowing particles to settle on a magnetic rack and removing supernatant. Rinsing was repeated three times. Acetonitrile (ACN, Sigma-Aldrich) was added to the protein sample and prepared particles to 77% final ACN concentration and incubated for 30 min at RT. Sample tubes were placed on a magnetic rack and incubated for a further 10 min at RT until supernatant ran clear. To remove the detergent from the magnetic particles, a

2-step 70% ethanol wash followed by 1-step ACN wash was performed until bubbles were no longer visible on the magnetic particles. Magnetic particles were reconstituted in trypsin:total protein digest ratio of 1:50 (from $0.2 \mu\text{g} \mu\text{l}^{-1}$ trypsin protease in acetic acid stock) overnight. The following day, sample tubes were added to the magnetic rack and peptide-containing supernatant was removed. Remaining peptides were removed from magnetic particles with 2% Dimethyl sulfoxide (Sigma-Aldrich) in MilliQ and incubated for 2 min at RT off the rack. Both supernatants were combined and acidified with 1 μl 10% formic acid (FA - reagent grade) prior to analysis on mass spectrometry.

Proteomics methods components

Desalted samples were separated on an UltiMate 3000 UHPLC system (Thermo Fischer Scientific, UK) and electro-sprayed directly into a Q-Exactive Mass Spectrometer (Thermo Fischer Scientific) through an EASY-Spray nano-electrospray ion source (Thermo Fischer Scientific). The peptides were trapped on a C18 Acclaim™ PepMap™ 100 pre-column ($300 \mu\text{m}$ i.d. \times 5 mm, 100 Å, Thermo Fisher Scientific) using solvent A (0.1% FA in MilliQ) at a pressure of 500 bar. The peptides were separated on an in-house packed analytical column ($75 \mu\text{m}$ i.d. \times 50 cm packed with ReproSil-Pur 120 C18-AQ, 1.9 μm , 120 Å, Dr. Maisch GmbH, Germany) using a linear gradient (length: 65 min, 15%–35% solvent B (0.1% FA in ACN), flow rate: 200 nl min^{-1}). Data were acquired in a data-dependent mode. Full scan MS spectra were acquired in the Orbitrap (scan range 350–1500 m/z , resolution 70 000, AGC target 3×10^6 , maximum injection time 50 ms^{-1}). The 3 or 20 most intense peaks were selected for HCD fragmentation at 30% of normalised collision energy (resolution 17 500, AGC target 5×10^4 , maximum injection time 120 ms^{-1}) with first fixed mass at 180 m/z . A Top 3 method (three MS/MS collected per MS scan) was used for the label-free quantitative comparisons while a separate run was performed using a Top 20 method for qualitative analysis.

Data analysis pipeline

Identification of peptides was performed using MaxQuant computational proteomics platform (version 1.5.3.30) with the implemented Andromeda algorithm (Cox and Mann, 2008; Wiśniewski *et al.*, 2013) by searching MS/MS spectra against a database consisting of the protein translation of the *N. maritimus* genome obtained from UniProt (<https://www.uniprot.org/proteomes/UP000000792>). Protein matches were filtered to an FDR of 1% at the peptide to spectrum match, peptide and protein levels. Measured

intensities were converted to LFQ intensities using MaxLFQ algorithm (Cox *et al.*, 2014) integrated within MaxQuant (using default parameters), using both unique and razor peptides for protein quantification. The MaxLFQ algorithm uses a non-linear optimisation model to normalise the peptide intensities thereby ensuring that profiles of LFQ intensities across samples accurately reflect the relative amounts of the proteins - taking into account all the peptide ratios for each protein measured in all pairwise comparisons of the different quantified samples and removing outliers (Cox *et al.*, 2014). Protein LFQ intensities do not equate to protein abundance, and therefore intensities of the same protein across treatments are only robustly comparable - intensities of different proteins within treatments cannot be accurately compared. Mean LFQ intensities for Fe-limited and Fe-replete treatments were calculated from replicates and tested for significant differences using a student's *t*-test at an FDR-adjusted *p*-value of 0.05 in Perseus software (version 1.5.1.6). All differentially intense proteins are listed in the Supplementary Table 1. No statistical analysis was performed for proteins which were absent or below the limit of detection, and instead a presence-absence response was assigned.

Biological function groups and Fe containing proteins

Biological function categories (Supplementary Table 1) were assigned to proteins using the Gene Ontology (GO database). Where GO terms were not available, we used the Kyoto Encyclopaedia of Genes and Genomes (Kanehisa *et al.*, 2007) reference pathways or InterPro to assign putative biological functions. In order to gain an insight into the effect of Fe limitation specifically on the Fe-containing proteome, we identified the Fe-containing proteins within the *N. maritimus* proteome. A full list of proteins encoded by the *N. maritimus* genome was downloaded from UniProt (proteome ID UP000000792) which was subsequently submitted to the PHYRE2 protein fold recognition server to identify homologues for known protein structures (Kelley *et al.*, 2009). Significant matches (>95% confidence) were submitted to metalPDB (Putignano *et al.*, 2018; Andreini *et al.*, 2012) which models the 3D minimal functional sites surrounding metals. Metals were assigned if the search returned significant sequence similarity to metal-binding sites in other proteins (*e*-value <10⁻⁵). This identification is underpinned by the assumption that the genome-predicted proteome of *N. maritimus* has been accurately annotated and that any archaeal proteins which are homologous to characterised bacterial Fe proteins also have similar Fe stoichiometry. By identifying homologues based on predicted 3D protein structures which are highly conserved, we have greater confidence that Fe stoichiometry will also be conserved.

Acknowledgements

We thank Phillip Holdship (Oxford) for ICP-MS technical assistance, Shabaz Mohammed (Oxford) and Sabrina Liberatori (Oxford) for assistance with sample preparation for proteomic analyses and interpretation of proteomic data. We also extend our gratitude to Christopher L. Dupont for comments which greatly improved the manuscript. This research was supported by funding from the UK Natural Environmental Research Council (NERC) and ERC Consolidator Grant APPELS: ERC-2015-COG-681746. We also acknowledge the Royal Society for a Wolfson Research Merit Award to RR.

References

- Allen, A.E., LaRoche, J., Maheswari, U., Lommer, M., Schauer, N., Lopez, P.J., *et al.* (2008) Whole-cell response of the pennate diatom *Phaeodactylum tricornutum* to iron starvation. *Proc Natl Acad Sci U S A* **105**: 10438–10443.
- Amin, S.A., Moffett, J.W., Martens-Habben, W., Jacquot, J. E., Han, Y., Devol, A., *et al.* (2013) Copper requirements of the ammonia-oxidizing archaeon *Nitrosopumilus maritimus* SCM1 and implications for nitrification in the marine environment. *Limnol Oceanogr* **58**: 2037–2045.
- Andreini, C., Cavallaro, G., Lorenzini, S., and Rosato, A. (2012) MetalPDB: a database of metal sites in biological macromolecular structures. *Nucleic Acids Res* **41**: D312–D319.
- Bayer, B., Pelikan, C., Bittner, M.J., Reinthaler, T., Könneke, M., Herndl, G.J., and Offe, P. (2019) Proteomic response of three marine ammonia-oxidizing archaea to hydrogen peroxide and their metabolic interactions with a heterotrophic alphaproteobacterium. *Msystems* **4**: e00181–19.
- Berg, G.M., Balode, M., Purina, I., Bekere, S., Béchemin, C., and Maestrini, S.Y. (2003) Plankton community composition in relation to availability and uptake of oxidized and reduced nitrogen. *Aquat Microb Ecol* **30**: 263–274.
- Boiteau, R.M., Mende, D.R., Hawco, N.J., McIlvin, M.R., Fitzsimmons, J.N., Saito, M.A., *et al.* (2016) Siderophore-based microbial adaptations to iron scarcity across the eastern Pacific Ocean. *Proc Natl Acad Sci U S A* **113**: 14237–14242.
- Chappell, P.D., Whitney, L.P., Wallace, J.R., Darer, A.I., Jean-Charles, S., and Jenkins, B.D. (2015) Genetic indicators of iron limitation in wild populations of *Thalassiosira oceanica* from the Northeast Pacific Ocean. *ISME J* **9**: 592–602.
- Clark, L.L., Ingall, E.D., and Benner, R. (1999) Marine organic phosphorus cycling; novel insights from nuclear magnetic resonance. *Am J Sci* **299**: 724–737.
- Cohen, N.R., Gong, W., Moran, D.M., McIlvin, M.R., Saito, M.A., and Marchetti, A. (2018) Transcriptomic and proteomic responses of the oceanic diatom *Pseudo-nitzschia granii* to iron limitation. *Environ Microb* **20**: 3109–3126.
- Cook, A.M., Daughton, C.G., and Alexander, M. (1978) Phosphate utilization by bacteria. *J Bacteriol* **133**: 85–90.

- Coves, J., Eschenbrenner, M., and Fontecave, M. (1993) Sulfite reductase of *Escherichia coli* is a ferrisiderophore reductase. *Biochem Biophys Res Commun* **192**: 1403–1408.
- Cox, J., and Mann, M. (2008) MaxQuant enables high peptide identification rates, individualized ppb-range mass accuracies and proteome-wide protein quantification. *Nat Biotechnol* **26**: 1367–1372.
- Cox, J., Hein, M.Y., Lubner, C.A., Paron, I., Nagaraj, N., and Mann, M. (2014) Accurate proteome-wide label-free quantification by delayed normalization and maximal peptide ratio extraction, termed MaxLFQ. *Mol Cell Proteomics* **13**: 2513–2526.
- Cunningham, B.R., and John, S.G. (2017) The effect of iron limitation on cyanobacteria major nutrient and trace element stoichiometry. *Limnol Oceanogr* **62**: 846–858.
- Doxey, A.C., Kurtz, D.A., Lynch, M.D., Sauder, L.A., and Neufeld, J.D. (2015) Aquatic metagenomes implicate Thaumarchaeota in global cobalamin production. *ISME J* **9**: 461–471.
- Dyhrman, S.T., Chappell, P.D., Haley, S.T., Moffett, J.W., Orchard, E.D., Waterbury, J.B., and Webb, E.A. (2006) Phosphonate utilization by the globally important marine diazotroph *Trichodesmium*. *Nature* **439**: 68–71.
- Erdner, D.L., Price, N.M., Doucette, G.J., Peleato, M.L., and Anderson, D.M. (1999) Characterization of ferredoxin and flavodoxin as markers of iron limitation in marine phytoplankton. *Mar Ecol Prog* **184**: 43–53.
- Fawcett, S.E., Lomas, M.W., Casey, J.R., Ward, B.B., and Sigman, D.M. (2011) Assimilation of upwelled nitrate by small eukaryotes in the Sargasso Sea. *Nat Geosci* **4**: 717–722.
- Feike, J., Jürgens, K., Hollibaugh, J.T., Krüger, S., Jost, G., and Labrenz, M. (2012) Measuring unbiased metatranscriptomics in suboxic waters of the central Baltic Sea using a new in situ fixation system. *ISME J* **6**: 461–470.
- Fourquez, M., Devez, A., Schaumann, A., Guéneuguès, A., Jouenne, T., Obernosterer, I., and Blain, S. (2014) Effects of Iron Limitation on Growth and Carbon Metabolism in Oceanic and Coastal Heterotrophic Bacteria. *Limnol Oceanogr* **59**: 349–360.
- Freing, A., Wallace, D.W., and Bange, H.W. (2012) Global oceanic production of nitrous oxide. *Philos Trans R Soc Lond B Biol Sci* **367**: 1245–1255.
- Fu, F.X., Mulholland, M.R., Garcia, N.S., Beck, A., Bernhardt, P.W., Warner, M.E., et al. (2008) Interactions between changing pCO₂, N₂ fixation, and Fe limitation in the marine unicellular cyanobacterium *Crocosphaera*. *Limnol Oceanogr* **53**: 2472–2484.
- Glibert, P.M., Wilkerson, F.P., Dugdale, R.C., Raven, J.A., Dupont, C.L., Leavitt, P.R., et al. (2016) Pluses and minuses of ammonium and nitrate uptake and assimilation by phytoplankton and implications for productivity and community composition, with emphasis on nitrogen-enriched conditions. *Limnol Oceanogr* **61**: 165–197.
- Gorman-Lewis, D., Martens-Habben, W., and Stahl, D.A. (2019) Cu (II) adsorption onto ammonia-oxidizing bacteria and archaea. *Geochim Cosmochim Acta* **255**: 127–143.
- Gorman-Lewis, D., Martens-Habben, W., and Stahl, D.A. (2014) Thermodynamic characterization of proton-ionizable functional groups on the cell surfaces of ammonia-oxidizing bacteria and archaea. *Geobiology* **12**: 157–171.
- Granger, J., and Price, N.M. (1999) The importance of siderophores in iron nutrition of heterotrophic marine bacteria. *Limnol Oceanogr* **44**: 541–555.
- Griess, P. (1879) Griess reagent: a solution of sulphanilic acid and α -naphthylamine in acetic acid which gives a pink colour on reaction with the solution obtained after decomposition of nitrosyl complexes. *Chem Ber* **12**: 427.
- Gustafsson, J.P. (2010) *Visual MINTEQ ver. 3.0*. URL <http://www.2.lwr.kth.se/English/OurSoftware/vminteq/index.htm>.
- Gutierrez, T., Biller, D.V., Shimmield, T., and Green, D.H. (2012) Metal binding properties of the EPS produced by *Halomonas* sp. TG39 and its potential in enhancing trace element bioavailability to eukaryotic phytoplankton. *Bio-metals* **25**: 1185–1194.
- Hassler, C.S., Norman, L., Nichols, C.A.M., Clementson, L.A., Robinson, C., Schoemann, V., et al. (2015) Iron associated with exopolymeric substances is highly bioavailable to oceanic phytoplankton. *Mar Chem* **173**: 136–147.
- Hassler, C.S., Schoemann, V., Nichols, C.M., Butler, E.C., and Boyd, P.W. (2011) Saccharides enhance iron bioavailability to Southern Ocean phytoplankton. *Proc Natl Acad Sci U S A* **108**: 1076–1081.
- Heal, K.R., Qin, W., Ribalet, F., Bertagnolli, A.D., Coyote-Maestas, W., Hmelo, L.R., et al. (2017) Two distinct pools of B12 analogs reveal community interdependencies in the ocean. *Proc Natl Acad Sci U S A* **114**: 364–369.
- Hogle, S.L., Thrash, J.C., Dupont, C.L., and Barbeau, K.A. (2016) Trace metal acquisition by marine heterotrophic bacterioplankton with contrasting trophic strategies. *Appl Environ Microbiol* **82**: 1613–1624.
- Hollibaugh, J.T., Gifford, S., Sharma, S., Bano, N., and Moran, M.A. (2011) Metatranscriptomic analysis of ammonia-oxidizing organisms in an estuarine bacterioplankton assemblage. *ISME J* **5**: 866–878.
- Holmes, K., Mulholland, F., Pearson, B.M., Pin, C., McNicholl-Kennedy, J., Ketley, J.M., and Wells, J.M. (2005) *Campylobacter jejuni* gene expression in response to iron limitation and the role of fur. *Microbiology* **151**: 243–257.
- Horecker, B.L., Tsolas, O., and Lai, C.Y. (1972) 6 Aldolases. In *The enzymes*, Vol. 7, Boyer, P.D. (ed). New York: Academic Press, pp. 213–258.
- Hughes, C.S., Moggridge, S., Müller, T., Sorensen, P.H., Morin, G.B., and Krijgsveld, J. (2019) Single-pot, solid-phase-enhanced sample preparation for proteomics experiments. *Nat Protoc* **14**: 68–85.
- Jang, S., and Imlay, J.A. (2010) Hydrogen peroxide inactivates the *Escherichia coli* Isc iron-sulphur assembly system, and OxyR induces the Suf system to compensate. *Mol Microbiol* **78**: 1448–1467.
- Kanehisa, M., Araki, M., Goto, S., Hattori, M., Hirakawa, M., Itoh, M., et al. (2007) KEGG for linking genomes to life and the environment. *Nucleic Acids Res* **36**: D480–D484.
- Karner, M.B., DeLong, E.F., and Karl, D.M. (2001) Archaeal dominance in the mesopelagic zone of the Pacific Ocean. *Nature* **409**: 507–510.

- Kelley, L.A., and Sternberg, M.J.E. (2009). Protein structure prediction on the Web: a case study using the Phyre server. *Nature Protocols* **4**: 363–371.
- Keyer, K., and Imlay, J.A. (1996) Superoxide accelerates DNA damage by elevating free-iron levels. *Proc Natl Acad Sci U S A* **93**: 13635–13640.
- Komori, K., Miyata, T., DiRuggiero, J., Holley-Shanks, R., Hayashi, I., Cann, I.K., *et al.* (2000) Both RadA and RadB are involved in homologous recombination in *Pyrococcus furiosus*. *J Biol Chem* **275**: 33782–33790.
- Könneke, M., Bernhard, A.E., José, R., Walker, C.B., Waterbury, J.B., and Stahl, D.A. (2005) Isolation of an autotrophic ammonia-oxidizing marine archaeon. *Nature* **437**: 543–546.
- Könneke, M., Schubert, D.M., Brown, P.C., Hügler, M., Standfest, S., Schwander, T., *et al.* (2014) Ammonia-oxidizing archaea use the most energy-efficient aerobic pathway for CO₂ fixation. *Proc Natl Acad Sci U S A* **111**: 8239–8244.
- Krapp, A.R., Tognetti, V.B., Carrillo, N., and Acevedo, A. (1997) The role of ferredoxin-NADP⁺ reductase in the concerted cell defense against oxidative damage: studies using *Escherichia coli* mutants and cloned plant genes. *Eur J Biochem* **249**: 556–563.
- Kustka, A.B., Allen, A.E., and Morel, F.M. (2007) Sequence analysis and transcriptional regulation of iron acquisition genes in two marine diatoms. *J Phycol* **43**: 715–729.
- La Roche, J., Boyd, P.W., McKay, R.M.L., and Geider, R.J. (1996) Flavodoxin as an in situ marker for iron stress in phytoplankton. *Nature* **382**: 802–805.
- Li, P.N., Herrmann, J., Tolar, B.B., Poitevin, F., Ramdasi, R., Bargar, J.R., *et al.* (2018) Nutrient transport suggests an evolutionary basis for charged archaeal surface layer proteins. *ISME J* **12**: 2389–2402.
- Liochev, S.I., and Fridovich, I. (1994) The role of O₂·⁻ in the production of HO· in vitro and in vivo. *Free Radic Biol Med* **16**: 29–33.
- Maldonado, M.T., Allen, A.E., Chong, J.S., Lin, K., Leus, D., Karpenko, N., and Harris, S.L. (2006) Copper-dependent iron transport in coastal and oceanic diatoms. *Limnol Oceanogr* **51**: 1729–1743.
- Martens-Habbena, W., Berube, P.M., Urakawa, H., José, R., and Stahl, D.A. (2009) Ammonia oxidation kinetics determine niche separation of nitrifying Archaea and Bacteria. *Nature* **461**: 976–979.
- Metcalf, W.W., Griffin, B.M., Cicchillo, R.M., Gao, J., Janga, S.C., Cooke, H.A., *et al.* (2012) Synthesis of methylphosphonic acid by marine microbes: a source for methane in the aerobic ocean. *Science* **337**: 1104–1107.
- Moore, C.M., Mills, M.M., Arrigo, K.R., Berman-Frank, I., Bopp, L., Boyd, P.W., *et al.* (2013) Processes and patterns of oceanic nutrient limitation. *Nat Geosci* **6**: 701–710.
- Nachin, L., Nannmark, U., and Nyström, T. (2005) Differential roles of the universal stress proteins of *Escherichia coli* in oxidative stress resistance, adhesion, and motility. *J Bacteriol* **187**: 6265–6272.
- Nyström, T., and Neidhardt, F.C. (1994) Expression and role of the universal stress protein, UspA, of *Escherichia coli* during growth arrest. *Mol Microbiol* **11**: 537–544.
- Ozdemir, G., Ozturk, T., Ceyhan, N., Isler, R., and Cosar, T. (2003) Heavy metal biosorption by biomass of *Ochrobactrum anthropi* producing exopolysaccharide in activated sludge. *Bioresour Technol* **90**: 71–74.
- Parks, D.H., Chuvochina, M., Chaumeil, P.A., Rinke, C., Mussig, A.J., and Hugenholtz, P. (2020) A complete domain-to-species taxonomy for Bacteria and Archaea. *Nat Biotechnol* **28**: 1–8.
- Peers, G., and Price, N.M. (2006) Copper-containing plastocyanin used for electron transport by an oceanic diatom. *Nature* **441**: 341–344.
- Picaud, S., Kavanagh, K.L., Yue, W.W., Lee, W.H., Muller-Knapp, S., Gileadi, O., *et al.* (2011) Structural basis of fumarate hydratase deficiency. *J Inher Metab Dis* **34**: 671–676.
- Price, N.M., Harrison, G.I., Hering, J.G., Hudson, R.J., Nirel, P.M., Palenik, B., and Morel, F.M. (1989) Preparation and chemistry of the artificial algal culture medium Aquil. *Biol Oceanogr* **6**: 443–461.
- Putignano, V., Rosato, A., Banci, L., and Andreini, C. (2018) MetalPDB in 2018: a database of metal sites in biological macromolecular structures. *Nucleic Acids Res* **46**: D459–D464.
- Qin, W., Amin, S.A., Lundeen, R.A., Heal, K.R., Martens-Habbena, W., Turkarslan, S., *et al.* (2018) Stress response of a marine ammonia-oxidizing archaeon informs physiological status of environmental populations. *ISME J* **12**: 508–519.
- Qin, W., Zheng, Y., Zhao, F., Wang, Y., Urakawa, H., Martens-Habbena, W., *et al.* (2020) Alternative strategies of nutrient acquisition and energy conservation map to the biogeography of marine ammonia-oxidizing archaea. *ISME J* **14**: 2595–2609.
- Raven, J.A. (1988) The iron and molybdenum use efficiencies of plant growth with different energy, carbon and nitrogen sources. *New Phytol* **109**: 279–287.
- Reyes, C., Hodgskiss, L.H., Kerou, M., Pribasniig, T., Abby, S.S., Bayer, B., *et al.* (2020) Genome wide transcriptomic analysis of the soil ammonia oxidizing archaeon *Nitrososphaera viennensis* upon exposure to copper limitation. *ISME J* **14**: 2659–2674.
- Rinke, C., Chuvochina, M., Mussig, A.J., Chaumeil, P.A., Waite, D.W., Whitman, W.B., *et al.* (2020) A rank-normalized archaeal taxonomy based on genome phylogeny resolves widespread incomplete and uneven classifications. *bioRxiv*. <https://www.biorxiv.org/content/10.1101/2020.03.01.972265v2>.
- Rodrigues-Oliveira, T., Belmok, A., Vasconcellos, D., Schuster, B., and Kyaw, C.M. (2017) Archaeal S-layers: overview and current state of the art. *Front Microbiol* **8**: 2597.
- Saito, M.A., McIlvin, M.R., Moran, D.M., Goepfert, T.J., DiTullio, G.R., Post, A.F., and Lamborg, C.H. (2014) Multiple nutrient stresses at intersecting Pacific Ocean biomes detected by protein biomarkers. *Science* **345**: 1173–1177.
- Saito, M.A., McIlvin, M.R., Moran, D.M., Santoro, A.E., Dupont, C.L., and Rafter, P.A. (2020). Abundant nitrite-oxidizing metalloenzymes in the mesopelagic zone of the tropical Pacific Ocean. *Nature Geoscience* **13**: 355–362.
- Santoro, A.E., Richter, R.A., and Dupont, C.L. (2019) Planktonic marine archaea. *Ann Rev Mar Sci* **11**: 131–158.

- Santoro, A.E., Dupont, C.L., Richter, R.A., Craig, M.T., Carini, P., McIlvin, M.R., et al. (2015) Genomic and proteomic characterization of "Candidatus Nitrosopelagicus brevis": an ammonia-oxidizing archaeon from the open ocean. *Proc Natl Acad Sci U S A* **112**: 1173–1178.
- Santoro, A.E., Sakamoto, C.M., Smith, J.M., Plant, J.N., Gehman, A.L., Worden, A.Z., et al. (2013) Measurements of nitrite production in and around the primary nitrite maximum in the Central California current. *Biogeosciences* **10**: 7395–7410.
- Sara, M., and Sleytr, U.B. (2000) S-layer proteins. *J Bacteriol* **182**: 859–868.
- Seitz, E.M., and Kowalczykowski, S.C. (2000) The DNA binding and pairing preferences of the archaeal RadA protein demonstrate a universal characteristic of DNA strand exchange proteins. *Mol Microbiol* **37**: 555–560.
- Sepúlveda Cisternas, I., Salazar, J.C., and García-Angulo, V.A. (2018) Overview on the bacterial iron-riboflavin metabolic axis. *Front Microbiol* **9**: 1478.
- Shafiee, R.T., Diver, P.J., Snow, J.T., Zhang, Q., and Rickaby, R.E.M. (2021). Marine ammonia-oxidising archaea and bacteria occupy distinct iron and copper niches. *ISME Communications* **1**: <http://doi.org/10.1038/s43705-021-00001-7>.
- Shafiee, R.T., Snow, J.T., Zhang, Q., and Rickaby, R.E.M. (2019) Iron requirements and uptake strategies of the globally abundant marine ammonia-oxidising archaeon, *Nitrosopumilus maritimus* SCM1. *ISME J* **13**: 2295–2305.
- Shi, D., Kranz, S.A., Kim, J.M., and Morel, F.M. (2012) Ocean acidification slows nitrogen fixation and growth in the dominant diazotroph *Trichodesmium* under low-iron conditions. *Proc Natl Acad Sci U S A* **109**: E3094–E3100.
- Shi, T., Sun, Y., and Falkowski, P.G. (2007) Effects of iron limitation on the expression of metabolic genes in the marine cyanobacterium *Trichodesmium erythraeum* IMS101. *Environ Microbiol* **9**: 2945–2956.
- Shiozaki, T., Ijichi, M., Isobe, K., Hashihama, F., Nakamura, K.I., Ehama, M., et al. (2016) Nitrification and its influence on biogeochemical cycles from the equatorial Pacific to the Arctic Ocean. *ISME J* **10**: 2184–2197.
- Shire, D.M., and Kustka, A.B. (2015) Luxury uptake, iron storage and ferritin abundance in *Prochlorococcus marinus* (Synechococcales) strain MED4. *Phycologia* **54**: 398–406.
- Snow, J.T., Polyviou, D., Skipp, P., Christmas, N.A., Hitchcock, A., Geider, R., et al. (2015) Quantifying integrated proteomic responses to iron stress in the globally important marine diazotroph *Trichodesmium*. *PLoS One* **10**: e0142626.
- Sunda, W.G., and Huntsman, S.A. (1995) Iron uptake and growth limitation in oceanic and coastal phytoplankton. *Mar Chem* **50**: 189–206.
- Urakawa, H., Martens-Habben, W., and Stahl, D.A. (2011) Physiology and genomics of ammonia-oxidizing archaea. In *Nitrification*, Ward, B.B., Arp, D.J., and Klotz, M.G. (eds). Washington, DC: ASM Press, pp. 117–155.
- Walker, C.B., De La Torre, J.R., Klotz, M.G., Urakawa, H., Pineda, N., Arp, D.J., et al. (2010) *Nitrosopumilus maritimus* genome reveals unique mechanisms for nitrification and autotrophy in globally distributed marine crenarchaea. *Proc Natl Acad Sci U S A* **107**: 8818–8823.
- Webb, E.A., Moffett, J.W., and Waterbury, J.B. (2001) Iron stress in open-ocean cyanobacteria (*Synechococcus*, *trichodesmium*, and *Crocosphaera* spp.): identification of the idia protein. *Appl Environ Microbiol* **67**: 5444–5452.
- Wilhelm, S.W., Maxwell, D.P., and Trick, C.G. (1996) Growth, iron requirements, and siderophore production in iron-limited *Synechococcus* PCC 72. *Limnol Oceanogr* **41**: 89–97.
- Wiśniewski, J.R., Duś, K., and Mann, M. (2013) Proteomic workflow for analysis of archival formalin-fixed and paraffin-embedded clinical samples to a depth of 10 000 proteins. *Proteomics Clin Appl* **7**: 225–233.
- Yingping, F., Lemeille, S., Talla, E., Janicki, A., Denis, Y., Zhang, C.C., and Latifi, A. (2014) Unravelling the cross-talk between iron starvation and oxidative stress responses highlights the key role of PerR (alr 0957) in peroxide signalling in the cyanobacterium *Nostoc* PCC 7120. *Environ Microbiol Rep* **6**: 468–475.
- Yool, A., Martin, A.P., Fernández, C., and Clark, D.R. (2007) The significance of nitrification for oceanic new production. *Nature* **447**: 999–1002.
- Zhang, Q., Snow, J.T., Holdship, P., Price, D., Watson, P., and Rickaby, R.E.M. (2018) Direct measurement of multi-elements in high matrix samples with a flow injection ICP-MS: application to the extended *Emiliania huxleyi* Redfield ratio. *J Anal At Spectrom* **33**: 1196–1191.

Supporting Information

Additional Supporting Information may be found in the online version of this article at the publisher's web-site:

Supplementary Fig. 1. Effect of Fe' on nitrite (NO₂⁻) production by *N. maritimus* SCM1

Supplementary Fig. 2. Log-log scatter plots of raw and LFQ intensities in Fe-replete (1050 pmol L⁻¹ Fe') and Fe-limited (250 pmol L⁻¹ Fe') replicate treatments showing reproducibility of biological replicates. Correlation coefficient (r²) values are shown on each plot.

Supplementary Fig. 3. Spectral counts of AMO subunits generated using the Ocean Protein Portal (Saito et al. 2020) from the ProteOMZ metaproteomic dataset (FK160115 cruise to the central Pacific Ocean). *Nitrosopumilus maritimus* AmoA (Nmar_1500), AmoB (Nmar_1503) and AmoC (Nmar_1502) FASTA sequences were used as search criteria to search against metaproteomic database.

Supplementary Fig. 4. Significant log₂ changes (5% FDR-adjusted p-value) in protein intensity in this study plotted against the log₂ fold change in that corresponding gene transcript under Cu limitation in Qin et al. (2018). Proteins in grey shaded area offset from x-axis represent proteins only detected in one of the Fe treatments. Proteins are grouped into their biological function groups. Labelled proteins/genes represent the following: AmoA: Nmar_1500, UspA: Nmar_1659, Sulphite reductase: Nmar_0679, PhnD: Nmar_0875, FLDX: Nmar_1356, Ferredoxins: Nmar_0239, Nmar_1537. Comparison of data shown in Supplementary Table.

Supplementary Fig. 5. Proteins showing significant changes (FDR-adjusted p-value <0.05) in LFQ intensities on a \log_2 fold scale assigned into different biological function groups. Bars reaching 'Fe-replete only' or 'Fe-limited only' indicate proteins which were only present under that treatment and absent from the contrasting treatment.

Supplementary Fig. 6. Schematic Figure showing two hypothetical pathways linking increased Phn intensity under Fe limitation with methylphosphonate production. Hypothesis 1: A) Under Fe-replete conditions, there is sufficient Fe to allow for the production of Fe-binding proteins methylphosphonate synthase and final step in *N. maritimus* methylphosphonate production. B) Under Fe limitation, there is not sufficient Fe to catalyse the final step and thus *N. maritimus* increases the uptake of exogenous phosphonates to supplement the reduction in endogenous phosphonates. Hypothesis 2: C) Under Fe-replete conditions, the proportion of methylphosphonate which decorates the exopolymeric substances (EPS) is low, due to the abundance of extracellular Fe. D) Under Fe-limited conditions, exogenous phosphonate uptake is designed to enhance the cell's own methylphosphonate production to increase the proportion of P-bearing groups on the EPS. In doing so, the

EPS becomes more chemically attractive to Fe, thus supplying more Fe to the cell's putative ferric reductase (FeRDX) and increasing Fe uptake to the cell.

Supplementary Fig. 7. Dissolved Fe (nmol kg^{-1}) from GEOTRACES Intermediate Data Product 2017; downloaded from <https://webodv.awi.de/geotraces> in Jan 2021.

Supplementary Fig. 8. Analysis of *phnD* biogeography from TARA oceans gene Atlas. Figures show mean *phnD* copies per cell normalized to the mean *amoA* copies per cell from the same TARA sample (each point represents a different TARA sample – full data in Supplementary Table). Left hand panel shows results grouped into ≤ 200 m and > 200 m for consistency of comparison with Qin *et al.* (2020) and right-hand panel shows the grouping based on TARA parameters (where surface and dissolved chlorophyll maximum, DCM, are ≤ 200 m and mesopelagic is > 200 m). Error bars show range, box shows the standard deviation and line shows the mean.

Supplementary Fig. 9. Protein yield ($\mu\text{g ml}^{-1}$) recovered from various protein extraction buffers.

Table S1. Supporting table.